Sensitivity analysis of homogeneous reactions for thermochemical conversion of biomass in a downdraft gasifier

Umesh Kumar and Manosh C. Paul*

Systems, Power & Energy Research Division, James Watt School of Engineering, University of Glasgow

Glasgow G12 8QQ, UK

Abstract

Biomass containing organic materials could come from a number of sources such as from agricultural residues, sustainable forests, waste food, and industry by-products. Also, being a renewable source of energy, it has the significant potential to reduce greenhouse gas emissions releasing from the fossil fuel based technologies. Therefore, energy from biomass is becoming a favourable technology to convert solid fuel to valuable gas and one of the effective approaches is gasification. In this research, a three dimensional (3D) computational fluid dynamics (CFD) steady-state thermochemical model is developed to simulate biomass (rubber wood) gasification in a downdraft gasifier. Simulated CFD model includes all the four zones (drying, pyrolysis, oxidation and reduction) of gasifer. For optimising the gasifier temperature and syngas composition, a sensitivity analysis of homogeneous oxidation reactions is carried out, with the model identifying the suitable kinetic reactions for gasification. Predicted CFD modelling results are compared with those from the kinetic modelling and experimental results, where a good agreement is obtained. The effect of gasifier temperature, equivalence ratio (ER) and biomass feed rate on the syngas production is studied. Further, the effect of volatile composition and rate of Boudouard reaction at different ERs along the gasifier height is investigated.

Keywords: Biomass gasification; CFD modelling; chemical kinetics; discrete phase model

* Corresponding author. Tel.: +44(0) 141 330 8466; *E-mail address:* Manosh.Paul@glasgow.ac.uk

1. Introduction

The world's total energy consumption is estimated to increase from 549 quadrillion Btu in 2012 to 815 quadrillion Btu in 2040. The energy demand has also been expected to increase by 48% by 2040 in line with the increase in the world population and economic development worldwide [1]. However, the energy demand sets against the simultaneous fossil fuels depletion and the widespread concern about the environmental impact of energy conversion systems, well recognised as the main cause of the greenhouse gases emissions. This thus has progressively brought to light the role of renewable energy sources [2, 3].

Biomass is one of the trustable renewable sources of energy, which could be used for sustainable power and heat generation. Biomass is an alternate source of energy against the gradual depletion of conventional fossil fuels [4]. Biomass gasification is a thermochemical conversion process, which converts solid fuel into useful gaseous (syngas). Partial oxidation process of biomass, taking place in gasification, results in the production of carbon monoxide, carbon dioxide, hydrogen, and methane. The thermochemical conversion process or syngas quality is affected by the gasifying agent supply such as air, oxygen, steam and mixture of both [6]. It also produces long chain molecules such as tar and inert ash [5].

In the literature, various mathematical models have been developed to investigate the gasification systems on different levels of accuracy and modelling depth. Generally, these mathematical models can be categorised into two parts namely thermodynamic equilibrium and non-equilibrium or kinetic models. Thermodynamic equilibrium modelling technique is based on the maximum yield syngas and equilibrium temperature by assuming that the chemical reactions reach the equilibrium. However, most of the equilibrium model in the literature only considered a single lumped reaction model or considered four zones as a single lumped zone for downdraft gasifier [7-11]. But, in a real chemical reactive system, it is difficult to achieve the equilibrium and these models are independent on the reactor design, therefore these models are only helpful for studying the effect of operating parameters [12]. In addition, an equilibrium model lacks of detailing information inside the gasifier like gas-solid interface, gasifier temperature and concentration profile.

While a non-equilibrium or a kinetic model accounts the chemical and physical properties along the gasifier height by assuming a vertical object, it still lacks in comprehensively understanding and real visualisation of the biomass gasification systems and also the effect of operating parameter and design parameter on the syngas production [13-15]. Therefore, to

further progress this research, advanced computational fluid dynamics (CFD) models are required.

A CFD model was developed for gasification of sawdust in entrained gasifier [16]. Two-dimensional (2D) CFD model investigated the gasification systems, however, in this model only the oxidation zone was considered [17]. A three-dimensional model (3D) CFD model was developed for fast pyrolysis of biomass in a fluidized bed reactor. In that study, the main focus was to study the pyrolysis phenomena and impact of operating parameter on the pyrolysis process [18]. Another 2D CFD model was developed for biomass fast pyrolysis in a fluidized bed reactor [19]. Liu et al. [20] established a 3D steady state model to simulate biomass gasification in a circulating fluidized bed (CFB) reactor.

In the literature, a limited number of CFD simulation model for downdraft gasifiers are found. Of particular interest is the two dimensional CFD model for biomass gasification in a downdraft gasifier presented in [21]. They considered the gasifier as a rectangular two-dimensional geometry, which obviously does not reflect the real structure of a downdraft gasifier. Recently, the authors developed a 2D CFD model for a downdraft gasifier for the gasification of rubber wood feedstock [22],[25]. In this study, a volatile break-up approach was used to calculate the volatile fractions from feedstock, and the effect of gasifier temperature and equivalence ratio (ER) on the gas syngas composition was studied [22]. A very few 3D CFD study on biomass gasification in downdraft gasifier is reported in the literature. Further, in the literature, a large number of reaction kinetics published for biomass gasification. Therefore, a detailed kinetic study is initially performed in this work to optimise the reaction kinetics for biomass gasification. Further, an attempt is made to develop a full-scale 3D CFD model for biomass gasification in a downdraft gasifier. In the gasification, chemical kinetics play an important role in developing the computational model. Therefore, several reaction kinetics for the oxidation of carbon monoxide, hydrogen and methane are investigated in predicting the optimum gasifier temperature and syngas composition, backed up by the experimental and other data sourced from the literature. This model has also a crucial role to play in further development of the chemical kinetics research for gasification and be useful for better understanding of the biomass gasification process and its design conditions.

2. Model description

Figure 1 shows a schematic diagram of a downdraft gasifier used for biomass gasification modelling.

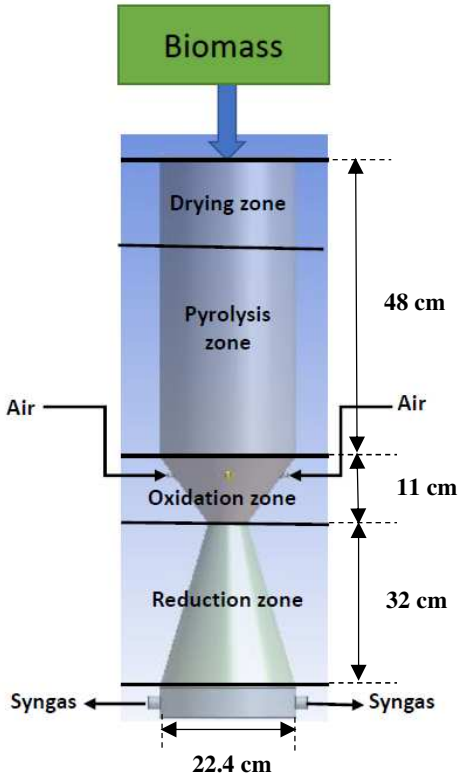

Figure 1. Schematic of the downdraft gasifier used for biomass gasification

The gasifier is divided into four zones namely drying, pyrolysis, oxidation and reduction, which are also shown in Figure 1. The dimensions as well as design conditions for the gasifier are taken from a recent study that focused on the development of an integrated kinetic model [23]. This kinetic model was tested with experimental results and subsequently, proposed the optimum design parameter for the downdraft gasifier used in this study. Air is injected from the oxidation zone while biomass is feed from the top of the gasifier.

The governing transport equations include the mass conservation, momentum transfer, energy and species concentrations which are solved numerically under the steady-state and turbulent flow conditions with a set of finite rate reaction kinetics as described below.

2.1 Mass and momentum conservation equations

The mass and momentum conservation equations respectively given as follows

$$\frac{\partial \rho}{\partial t} + \frac{\partial (\rho u_i)}{\partial x_i} = S_i \,, \tag{1}$$

where ρ is the density of fluid, u_i is the fluid velocity component and S_i is the mass element added to the continuous phase from the dispersed phase explained in Section 2.3.

$$\frac{\partial(\rho u_i)}{\partial t} + \frac{\partial(\rho u_i u_j)}{\partial x_j} = -\frac{\partial P}{\partial x_j} + \frac{\partial \tau_{ij}}{\partial x_j} + \rho g_i + F_i \,, \tag{2}$$

where g_i is the gravitational acceleration, P is the pressure, F_i is the external body force and τ_{ij} is the stress tensor expressed by the following equation

$$\tau_{ij} = \mu\left[\left(\frac{\partial u_i}{\partial x_j} + \frac{\partial u_j}{\partial x_i}\right) - \frac{2}{3}\nabla . u_{ij} I\right], \tag{3}$$

where μ is the molecular viscosity and I is the unit tensor that is associated with the effect of any volume dilation.

A Reynolds time-averaging technique is employed to first derive the Reynolds averaged Navier–Stokes (RANS) form of the equations from (1)-(3). The additional Reynolds stresses introduced in those equations are then modelled through the Boussinesq hypothesis depending strongly on the turbulence kinetic energy, k, and its rate of dissipation, ε, which are obtained from the following transport equations (standard k-ε model):

$$\frac{\partial}{\partial x_i}(\rho k u_i) = \frac{\partial}{\partial x_j}\left[\left(\mu + \frac{\mu_t}{\sigma_k}\right)\frac{\partial k}{\partial x_j}\right] + G_k + G_b - \rho\varepsilon - Y_M + S_k \,. \tag{4}$$

In the above equation, μ_t is the turbulent viscosity, σ_k is the turbulent viscosity, G_k is the turbulence kinetic energy due to the mean velocity gradients, G_b is the turbulence kinetic energy due to the buoyancy force, Y_M is the contribution of the fluctuating dilatation turbulence to the overall dissipation rate, and S_k is the source term for the kinetic energy.

$$\frac{\partial}{\partial x_i}(\rho\varepsilon u_i) = \frac{\partial}{\partial x_j}\left[\left(\mu + \frac{\mu_t}{\sigma_\varepsilon}\right)\frac{\partial \varepsilon}{\partial x_j}\right] + C_{1\varepsilon}\frac{\varepsilon}{k}(G_k + C_{3\varepsilon}G_b) - C_{2\varepsilon}\rho\frac{\varepsilon^2}{k} + S_\varepsilon \,, \tag{5}$$

where σ_ε is the turbulent Prandtl number for ε, and S_ε is the source term for the rate of dissipation. In equations (4) and (5), the model parameters used are $C_{1\varepsilon}$=1.44; $C_{2\varepsilon}$=1.92; σ_k=1.0; σ_ε=1.3 [24].

2.2 Species transport equation

The species transport equation is written as follows

$$\frac{\partial}{\partial t}(\rho Y_i) + \nabla.(\rho\vec{u}Y_i) = -\nabla.\vec{J}_i + R_i + S_i \,, \tag{6}$$

where Y_i is the mass fraction of species i, R_i is the net rate of production of species i by the chemical reaction, and J_i is the diffusion flux for turbulent flow expressed as

$$\vec{J_i} = -\left(\rho D_{i,m} + \frac{\mu_t}{Sc_t}\right)\nabla Y_i - D_{T,i}\frac{\nabla T}{T}, \quad (7)$$

where $D_{i,m}$ is the mass diffusion coefficient for species i in the mixture and $D_{T,i}$ is the thermal diffusion coefficient for species i. Sc_t is the Schmidt number for turbulent flow which is given by the following equation:

$$Sc_t = \frac{\mu_t}{\rho D_t} \quad (8)$$

In the above equation, D_t is the turbulent diffusivity.

2.3 Model for discrete phase

The flow of biomass particles is modelled by a Lagrangian approach namely discrete phase model (DPM). The model considers the trajectory of a particle through the continuous phase of fluid, while their interaction is accounted by considering the heat and mass losses of the particles as a source term in the governing equations. The trajectory of a discrete phase particle is written in a Lagrangian reference frame by integrating the force balance on the particle. This force balance equates the particle inertia with the forces acting on the particle as described by the following equation:

$$\frac{\partial \vec{u}_p}{\partial t} = F_D\left(\vec{u} - \vec{u}_p\right) + \frac{\vec{g}(\rho_p - \rho)}{\rho_p}, \quad (9)$$

where $\vec{u}_p$ is the particle velocity, $F_D\left(\vec{u} - \vec{u}_p\right)$ is the drag force per unit particle mass, ρ_p is the density of particle, and F_D is the drag force determined by

$$F_D = \frac{18\mu C_D Re}{24\rho_p {d_p}^2}, \quad (10)$$

where C_D is the drag coefficient, and the flow Reynolds number (Re) is derived by the following equation:

$$Re = \frac{\rho d_p |u - u_p|}{\mu}. \quad (11)$$

The kinetic devolatilization rate expression for the two competing rates (Kobayashi) model [24] is as given by the following equation:

$$\frac{m_v(t)}{(1-f_{w,0})m_{p,0}} = \int_0^t (\alpha_1 R_1 - \alpha_2 R_2)\left(exp\left(-\int_0^t (R_1 - R_2)dt\right)\right)dt\,, \quad (12)$$

where $m_v(t)$ is the volatile yield, $f_{w,0}$ is the mass fraction of biomass, $m_{p,0}$ is the initial particle mass at the injection boundary condition. R_1 and R_2 are the competing rates that control the devolatilization over various temperature range [24]:

$$R_1 = A_1 e^{-\frac{E}{RT}}\,, \quad (13)$$

$$R_1 = A_2 e^{-\frac{E}{RT}}\,, \quad (14)$$

where α_1, α_2 are the yield factors, and the value of α_1 is the mass fraction of volatile determined through the proximate analysis and α_2 is set as 1. Heat transfer during the devolatilization process are determined by the following equation

$$m_p c_p \frac{dT_P}{dt} = hA_P(T - T_P) + \frac{dm_P}{dt} h_{fg} + \varepsilon_P A_P \sigma\left({T_R}^4 - {T_P}^4\right), \quad (15)$$

where m_P is the mass of particle (kg), and c_p is the heat capacity of the particle (J/kg.K), T_P is the temperature of particle (K), h is the convective heat transfer coefficient (W/m^2.K), A_P is the surface area of the particle (m^3), h_{fg} is the latent heat (J/kg), ε_P is the particle emissivity, σ is the Stefan Boltzmann constant $(5.67 \times 10^{-8}\, kg\, s^{-3} K^{-4})$ and T_R is the radiation temperature (K). After the devolatilization process, char is formed and also volatile gases formed. Therefore, heat transfer during the char combustion / gasification process is derived by the following equation

$$m_P c_p \frac{dT_p}{dt} = hA_P(T - T_P) + f_h \frac{dm_p}{dt} H_{reaction} + \varepsilon_P A_P \sigma\left({T_R}^4 - {T_P}^4\right). \quad (16)$$

Finally, the particle temperature, convective heat transfer, and the absorption/emission of radiation of the particle surface are related by the following equation,

$$m_P c_p \frac{dT_p}{dt} = hA_p(T - T_P) + \varepsilon_p A_P \sigma\left({T_R}^4 - {T_P}^4\right). \quad (17)$$

3. Models for biomass gasification: thermochemical kinetics

3.1 Reaction for pyrolysis

Pyrolysis is a thermochemical process that occurs in the absence of oxygen. Biomass (rubber wood in this case) fed into the gasifier first decomposes into char, volatile gases and tar:

$$Rubber\ wood\ (CH_{1.54}O_{0.62}) \rightarrow Char + Volatile + Tar \quad (18)$$

To calculate the volatile species, a volatile break-up scheme was used in our previously published work [22, 25]. The model assumed that the volatile from biomass, consisting of carbon, hydrogen, oxygen, nitrogen and sulphur, converted to pseudo gas phase species, referred to as volatile using the devolatilization model:

$$Volatile \rightarrow x_{CO}CO + x_{CO_2}CO_2 + x_{H_2}H_2 + x_{CH_4}CH_4 + x_{H_2O}H_2O \quad (19)$$

However, tar is not considered in the CFD modelling due to its complex nature and remains outwith of the scope of this study. In reaction (19), the Stoichiometric coefficients x_{CO}, x_{CO_2}, x_{H_2}, x_{CH_4} and x_{H_2O} for the resultant species are calculated from the mass fractions obtained through the ultimate and proximate analysis data, shown in Table 1, and considering the molecular weights of these species.

Table 1. Chemical analysis data of rubber wood feedstock [26]

Proximate analysis (wt % dry basis)	
Volatile matter	81.1
Fixed carbon	19.2
Ash	0.7
Moisture content (wt % wet basis)	18.5
Ultimate analysis (wt% dry basis)	
C	50.6
H	6.5
O	42
N	0.2
S	0
Higher heating value (kJ/kg)	20540

3.2 Heterogeneous (char) reactions

After devolatilization, char reacts with other volatile gases released from feedstock as well as with oxygen, which takes place in the oxidation zone. These reactions (R1-R4) are exothermic however, except the carbon oxygen reaction (combustion/oxidation reaction), the entire heterogeneous reactions take place in the reduction zone.

$$C + 0.5O_2 \rightarrow CO \quad (R1)$$

$$C + CO_2 \rightarrow 2CO \quad (R2)$$

$$C + H_2O \rightarrow CO + H_2 \quad (R3)$$

$$C + 2H_2 \rightarrow CH_4 \quad (R4)$$

Table 2. Kinetics for the heterogeneous reactions [27]

Reactions	*A*	*E* (kJ/mol)	Temp(exponent)
R1: Partial oxidation	147000	112.99	1
R2: Boudouard Reaction	8.268	188.2	1
R3: Char-steam reaction	8.268	188.2	1
R4: Methanation reaction	8.88e-06	67.16	1

3.3 Homogenous reactions

For the gas phase reaction, CO, CO_2, CH_4, H_2, N_2 and O_2 species are included in the simulation model, as presented below.

$$CO + 0.5O_2 \rightarrow CO_2 \quad (R5)$$

$$H_2 + 0.5O_2 \rightarrow H_2O \quad (R6)$$

$$CH_4 + 1.5O_2 \rightarrow CO + 2H_2O \quad (R7)$$

$$CO + H_2O \rightarrow CO + H_2 \quad (R8)$$

$$CO + H_2 \rightarrow CO + H_2O \quad (R9)$$

$$CH_4 + H_2O \rightarrow CO + 3H_2 \quad (R10)$$

Table 3. Reaction kinetics for the homogeneous reactions [27, 28]

Reactions	*A*	*E* (kJ/mol)	Temp(exponent)
Oxidation of CO	2.32e+12	167	0
Oxidation of H_2	5.16e+13	28.5	0
Steam reforming reaction	2.8e+09	203	0
Water gas shift reaction	2.35e+10	288	0
Water gas shift reaction	1.78e+12	326	0
Methane reforming reaction	3.00e+05	125	0

3.4 Numerical methods and simulation setup

The boundary conditions (mass flow inlet, pressure outlet, isothermal wall) for the simulations are the same as those used in the kinetic model [23]. The 3D CAD design and mesh domain of downdraft gasifier are shown in Figure 2.

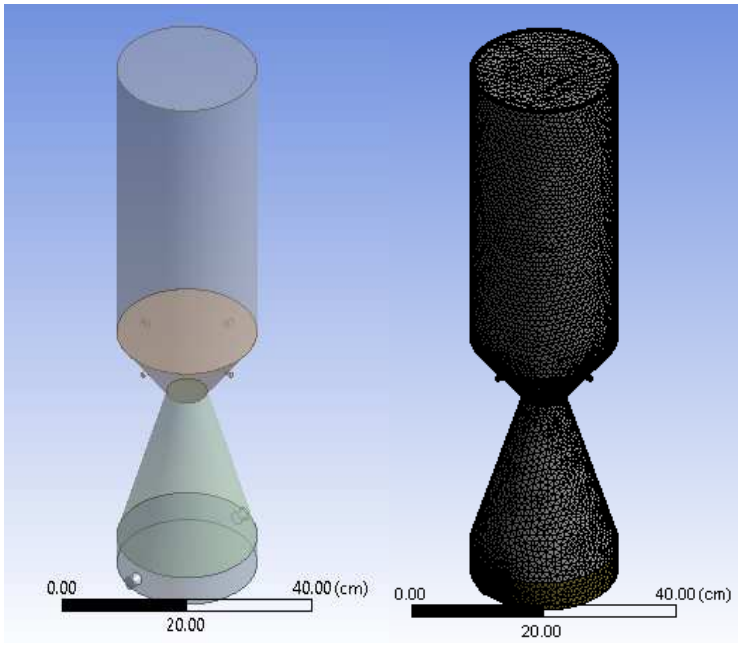

Figure 2 3D CAD design of downdraft gasifier and mesh domain

The operating conditions for the CFD simulation model are also shown in Table 4.

Table 4. Operating conditions for the CFD model

Operating conditions	
Air flow rate ($N.m^3/hr$)	1.64
Biomass feed rate (kg/hr)	3.65
Equivalence ratio (ER)	0.30-0.45
Pressure (atm)	1
Inlet air temperature (K)	600
Biomass feed temperature (K)	300

4. Results and discussion

As discussed above, CFD has been used to study the rubber wood gasification with the Eulerian-Lagrangian approach. Standard *k-ε* model is used to take into account the gas phase turbulence while the DPM model to take into account the solid phase interactions. Initially, a CFD model is established according to the above simulation setup. The developed model is then validated by using the data from the experiment [26] and kinetic model [23]. Further, the study is extended to investigate the effects of various operating variables such as the gasifier temperature and equivalence ratio on the producer gas compositions (CO, CH_4, CO_2, H_2, N_2).

4.1 Grid independence test

Initially, a grid dependency on the simulated results has been performed considering a computational grid cell of 215,012, 292,325, 418,685 and 666,707 respectively. The variation shown on the predicted results in Figure 3 is very moderate, and in fact, a negligible difference is observed between the results obtained by 215,012 and 292,325. Hence, the grid of 215,012 is deemed to be a suitable one and thus chosen for all the other simulation cases presented in the following sections.

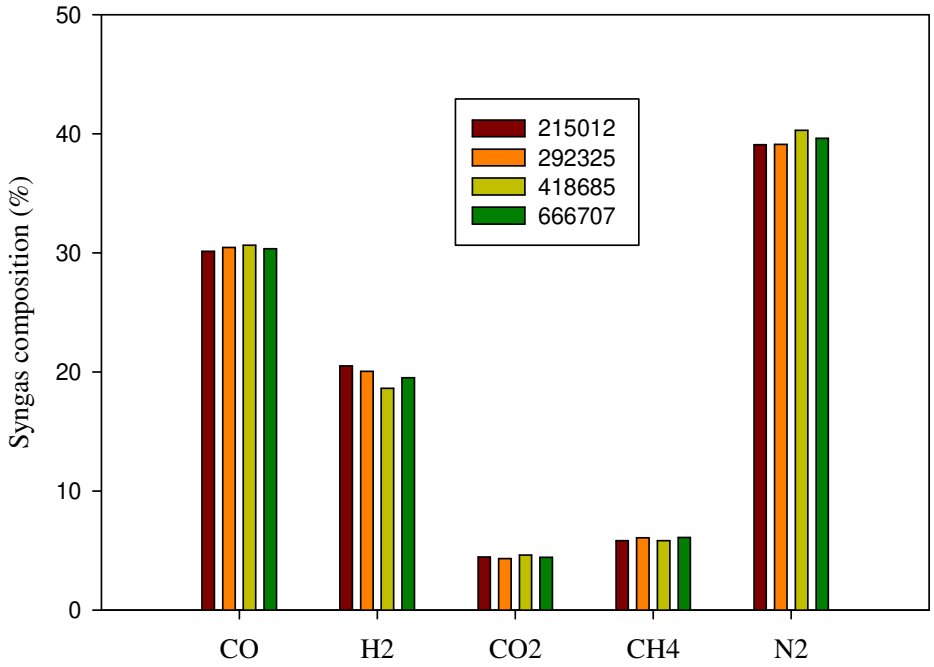

Figure 3 Gas compositions at the gasifier outlet for different mesh sizes

4.2 Cold flow analysis

Before looking into the gasification process in the gasifier, first, a cold flow simulation is performed to check the flow velocity distribution (i.e. the hydrodynamics) and the fluid flow pattern inside the gasifier. The flow velocity magnitude and velocity vector distributions inside the downdraft gasifier are shown in Figure 4.

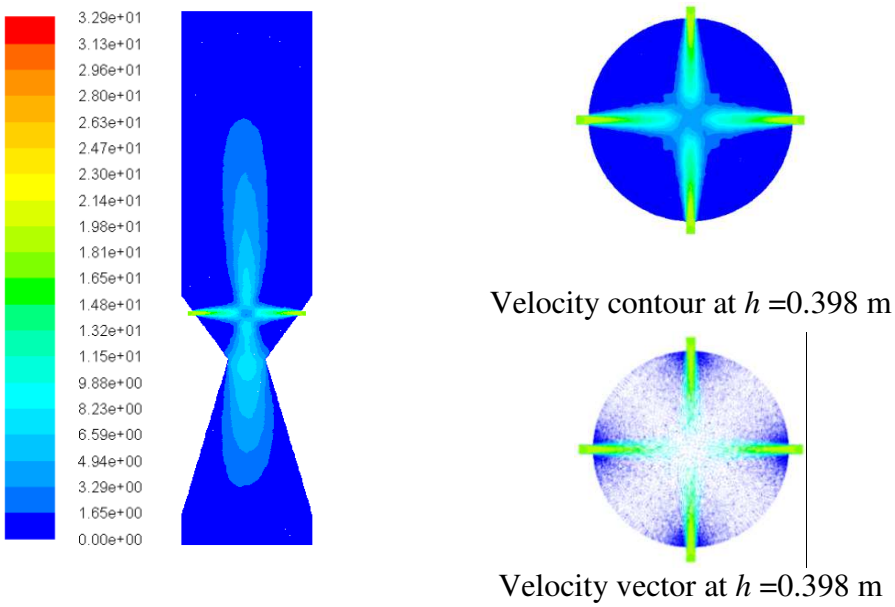

Figure 4. Velocity magnitude and velocity vector distributions inside the downdraft gasifier

For the injection of air, four nozzles are used as shown in Figure 4, and the maximum air velocity is found at the entrance of the air nozzles. All the air released from the nozzles is directed towards the centre of the gasifier, and the velocity vectors also show that the air velocity magnitude near the nozzle of the wall is very less due to the wall boundary conditions employed. Following the understanding of the flow physics from the cold flow simulation, the energy conservation and species transport equations are included and solved simultaneously.

4.3 Optimisation of the reaction kinetics for the homogeneous reactions

All the homogeneous reaction kinetics (Table 3) implemented into the CFD model result in the significant over-prediction of temperature inside the oxidation zone of the gasifier due to the exothermic nature of these reactions. This is a stumbling block for the CFD model to progress any further and hence, an in-depth sensitivity study on the kinetic parameters of the homogenous reactions is deemed to be crucial in this respect. Literature [28] suggests various reaction kinetic parameters for the homogeneous reactions (A and E) as shown in Table 5, having a further variation in the frequency factor and activation energy even for the same reaction. Figure 5 (a) shows the Arrhenius plots for the CO oxidation for the different chemical kinetics namely R5.1 to R5.5. This figure clearly points out the large discrepancies between one set of kinetics to another set. A close examination of Figure 5 (a) also reveals that the lowest value of ln(k) is obtained by R5 and highest for R5.4. Further, Reaction R5 needs lower activation energy to trigger the reaction compared to that of R5.4. Similarly, the

Arrhenius plots for the combustion of hydrogen and methane and the steam methane reforming are respectively presented in Figure 5(b), Figure 5(c) and Figure 5(d).

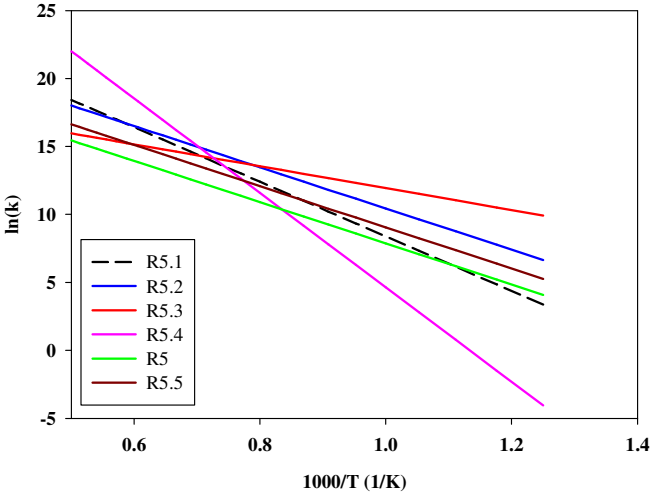

(a) Reaction kinetics for the oxidation of CO

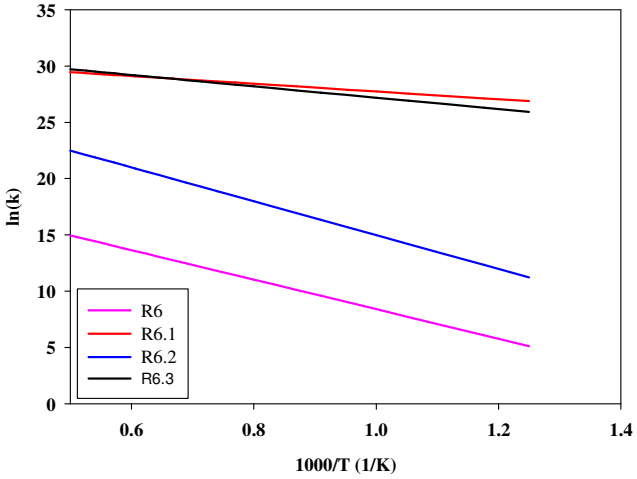

(b) Reaction kinetics for the formation of H_2O

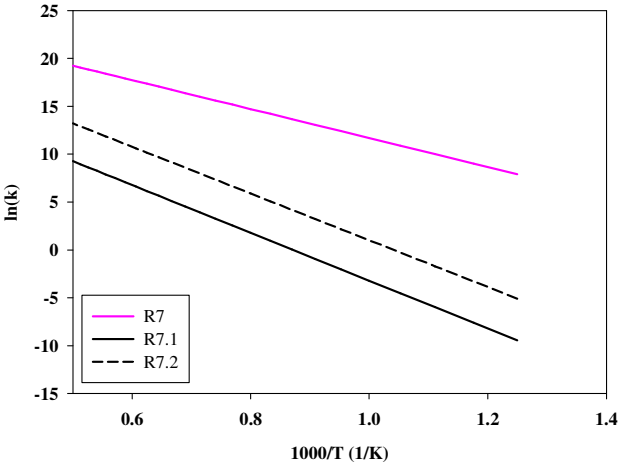

(c) Reaction kinetics for the oxidation of CH_4

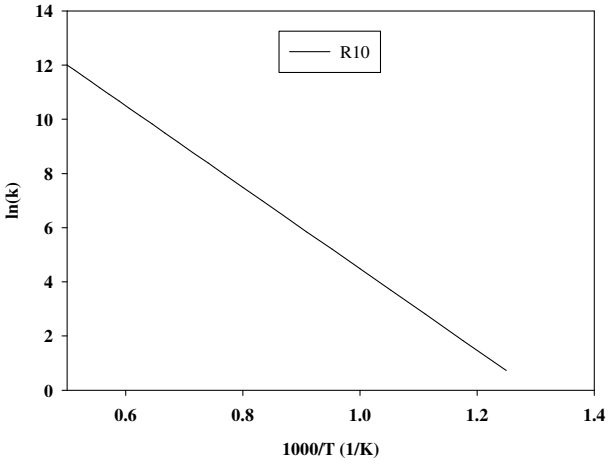

(d) Reaction kinetics for the steam reforming reaction

Figure 5. Arrhenius rate coefficients for different reactions

Again, the effects of the kinetic parameters on the reaction rates for the hydrogen and methane combustion and the way the order of these reactions are controlled, based on the data sourced from the literature, are clearly evidenced through these results. This is further examined through the CFD model and the simulated results in terms of the maximum temperature are presented in Figure 6.

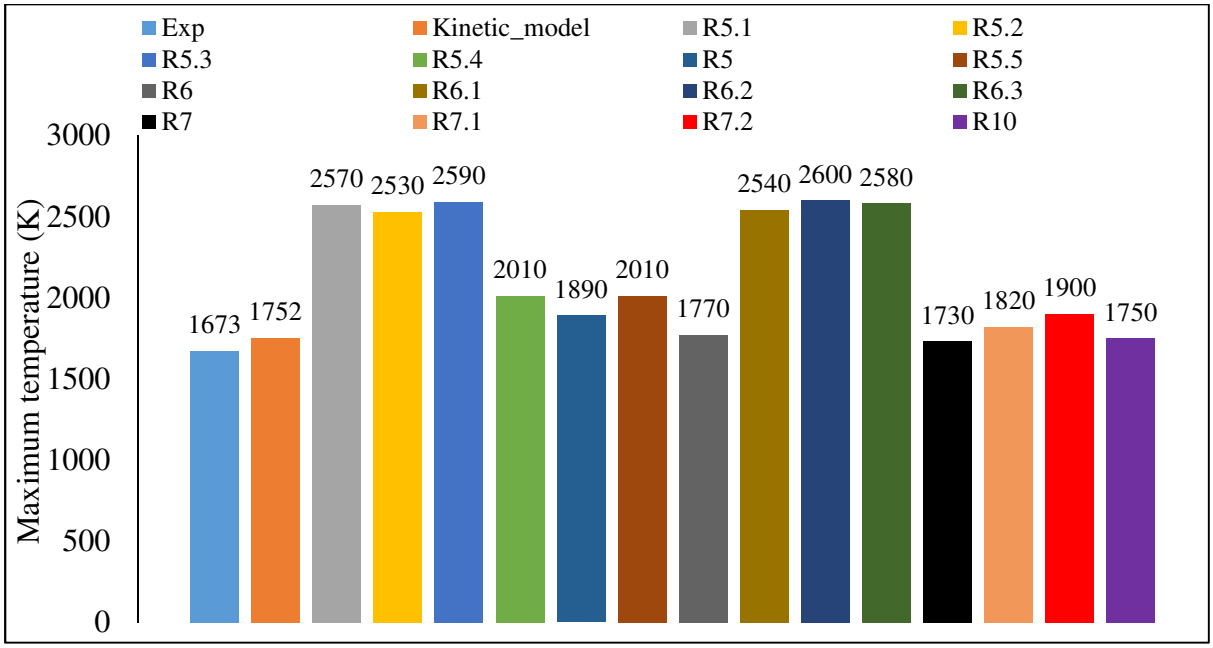

Figure 6. Maximum temperature inside the downdraft gasifier for different reaction kinetics

It is understood that the maximum heat release from the homogeneous reactions ocurs thorugh the combustion of carbon monoxide. So, the investigation is firstly focused on the kinetics of this particular reaction with additional five different set of reaction paratemers for R5.1 to R5.5 as shown in Table 5.

Table 5. Reaction kinetics for various reactions

Reaction kinetics for the oxidation of CO						
$CO + 0.5O_2 \rightarrow CO_2$; $r = Ae^{-E_a/(RT)} c_{CO}^{x} c_{O_2}^{y} c_{H_2O}^{z}$						
	x	y	z	E_a (kJ/mol)	A	Ref.
R5	1	0.5	0.5	126	1×10^{10}	[28]
R5.1	1	0.25	0.5	167	2.32×10^{12}	[29]
R5.2	1	0.5	0.5	126	1.30×10^{11}	[30]
R5.3	1	0.3	0.5	66.9	4.78×10^{8}	[31]
R5.4	1	0.25	0.5	289	1.28×10^{17}	[32]
R5.5	1	0.5	0.5	126	3.25×10^{10}	[33]
Reaction kinetics for the formation of H_2O						
$H_2 + 0.5O_2 \rightarrow H_2O$; $r = AT^{z} e^{-E_a/(RT)} c_{H_2}^{x} c_{O_2}^{y}$						
	x	y	z	E_a (kJ/mol)	A	Ref.
R6	1	1	0	109	2.20×10^{9}	[34]

R6.1	1.5	1	-1.5	28.5	5.16×10^{13}	[28]
R6.2	1	1	0	125	1.08×10^{13}	[35]
R6.3	1	1	0	42	1.0×10^{14}	[14]
Reaction kinetics for the oxidation of CH_4						
R7: $CH_4 + 0.5O_2 \rightarrow \mathrm{CO} + 2\mathrm{H_2}$ R7.1: $CH_4 + 1.5O_2 \rightarrow \mathrm{CO} + 2\mathrm{H_2O}$; $r = AT^z e^{-E_a/(RT)} c_{CH_4}^x c_{O_2}^y$ R7.2: $CH_4 + 2O_2 \rightarrow CO_2 + 2\mathrm{H_2O}$						
	x	*y*	*z*	E_a (kJ/mol)	*A*	Ref.
R7	0.5	1.25	0	126	4.40×10^{11}	[36]
R7.1	-0.3	1.3	0	203	2.80×10^{9}	[37]
R7.2	-0.3	1.3	0	203	1.10×10^{9}	[37]
Reaction kinetics for the methane reforming reaction						
$CH_4 + H_2O \rightarrow \mathrm{CO} + 3\mathrm{H_2}$; $r = AT^z e^{-E_a/(RT)} c_{CH_4}^x c_{H_2O}^y$						
	x	*y*	*z*	E_a (kJ/mol)	*A*	Ref.
R10	1	1	0	125	3.00×10^{8}	[36]

Further, from Figure 6 it is observed that the highest maximum temperature in the oxidation zone is achieved from reaction R6.2, which is 2600 K. This temperature outcome is indeed very high for biomass gasification. To further investigate the consequence on the gasification temperature, different sets of reaction kinetics first for the oxidation of CO (R5- R5.5, as in Table 5) are simulated and the oxidation temperature is compared alongside. As shown in Figure 6 again that the best agreed temperature result is obtained by R5 and in this context, this is considered to the optimised oxidation reaction for CO. Keeping this, the similar procedures were followed for the formation of water (R6 to R6.3) and oxidation of methane (R7 to R7.2). In addition, the steam reforming reaction was also included in the simulation, resulting in the optimised set of reaction kinetics that has the best agreed temperature. Table 6 finally presents these optimised reaction kinetics for the homogenous reactions.

Table 6. Optimised reaction kinetics for the homogenous reactions

Optimised Reactions	***A***	***E* (kJ/mol)**	**Temp(exponent)**
R5: Oxidation of CO	1e+10	126	0

R6: Oxidation of H_2	2.2e+09	109	0
R7: Steam reforming reaction	4.4e+11	126	0
R10: Methane reforming reaction	3.0e+08	125	0

The temperature distributions inside the whole gasifier are presented in Figure 7, as a set of contour plots, along both the radial and axial directions to assess the entire thermal field of the reactor.

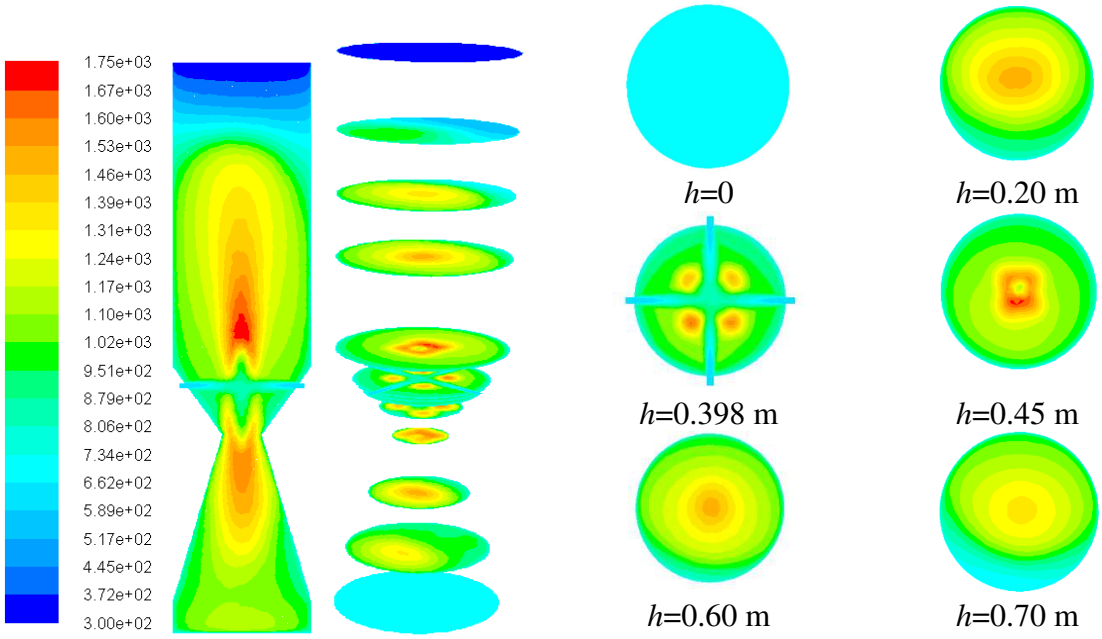

Figure 7. Temperature profiles inside the downdraft gasifier

As seen, the high-temperature regions are located at the oxidation zone due to the combustion reactions occurring above the air inlets, where the oxygen supply was adequate for combustion. The volatile gases, released from the pyrolysis zone, react with the oxygen available in this zone, and thus the maximum temperature zone is located there and the temperature near the air-nozzle regions is predicted to be lower. At the bottom of the gasifier (i.e. at h=0), the temperature range is 650-800 K which is a typical temperature of the gas releasing from the end of the reduction zone. While, towards the top of the gasifier, the temperature drops due to the heat required for both pyrolysis and drying of the biomass fed from the top of the gasifier initially at 300K.

Figure 8 presents a comparison of the simulated outlet composition of gases (CO, CO_2, H_2, CH_4, and N_2) with those obtained by the experimental testing and kinetic model results. These plots reveal that the simulated values of the outlet gas composition derived by the CFD model overestimate the gas composition of CO and CH_4; whereas the comparison of H_2 and CO_2 seems to be reasonable with an underproduction of N_2. The model, however, does not include any tar species content and hence thought to possibly have some impacts on the overall comparison of the gas species as presented in this figure.

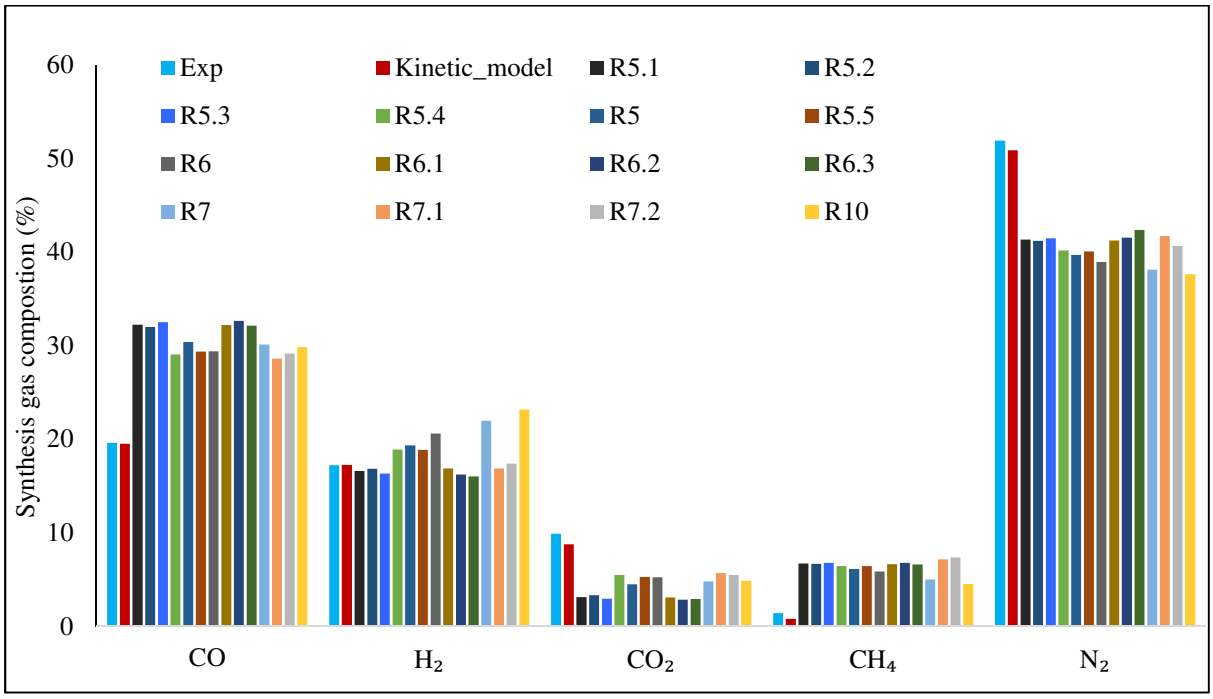

Figure 8. Syngas compositions for different reaction kinetics

The model, therefore, converted all the tar contents with impurities into the syngas components, resulting the predicted gas composition of CO and CH_4 higher than those in the experimental and kinetic model. These findings corroborate with the results available in the literature [21]. Further, nitrogen presents in air as an inert gas and due to that, nitrogen does not take part in any reaction process during the gasification. In the biomass gasification, some nitrogen is liberated by pyrolysis, whereas in gas combustion, nitrogen oxides are formed from some of the nitrogen compounds at temperature higher than that in gasification. Therefore, the unreactive nitrogen is passed through the gasification outlets with the producer gases and subsequently has an impact on the calorific value of the gases.

4.4 Effects of operating parameters

In the biomass gasification, equivalence ratio is one of the most important operating parameters used to predict the process performance and design of gasifier. Figure 9 illustrates the temperature profile along the gasifier height in the downdraft gasifier simulated at different equivalence ratios (ERs) changing from 0.30 to 0.45 at a constant biomass feed rate of 3.65 kg/hr. As seen in Figure 9, when the value of ER increases, the oxidation temperature increases due to an increase in the oxygen concentration. Subsequently, the char combustion and volatile combustion reactions (all are the exothermic reactions) are triggered and as a result, temperature increases.

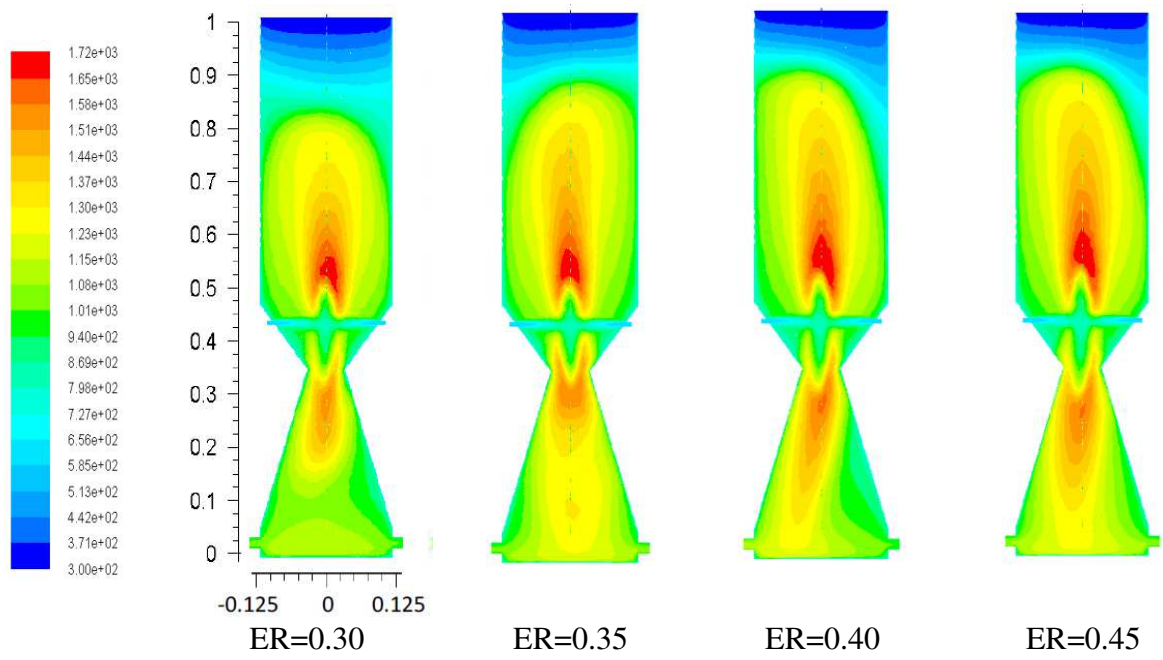

Figure 9. Temperature distribution in the downdraft gasifier at various ER

The predicted temperature was also in good agreement with that of the previously published results in the literature [38]. However, a significant drop in the temperature is examined in the pyrolysis zone. Drying and pyrolysis zone reactions are endothermic with a deficiency of heat. This heat deficiency recovers from the oxidation zone. Therefore, the process is linked with the endothermic drying, pyrolysis zone, and exothermic oxidation zone. In the oxidation zone, temperature increases and eventually becomes the highest due to the exothermic reactions occurring in this zone. In the reduction zone, mainly the endothermic reactions occur and, due to this, the temperature in the reduction zone drops.

Moreover, as seen in Figure 10, the quality of gas obtained from the gasifier also strongly depends on the ER value. However, a relatively low value of the equivalence ratio may result in many problems, e.g. it may lead to a low heating value of gases produced with an excessive amount of char formation thus further resulting in an incomplete gasification. On the other side, a too large value of equivalence ratio may result in an excessive formation of products through a complete combustion process. A close examination in Figure 10 further shows that the methane mole fraction decreases with an increase of the equivalence ratio. However, on the other side, the mole fraction of carbon dioxide increases with the equivalence ratio due to combustion, while the mole fraction of both carbon monoxide and hydrogen decreases with the equivalence ratio.

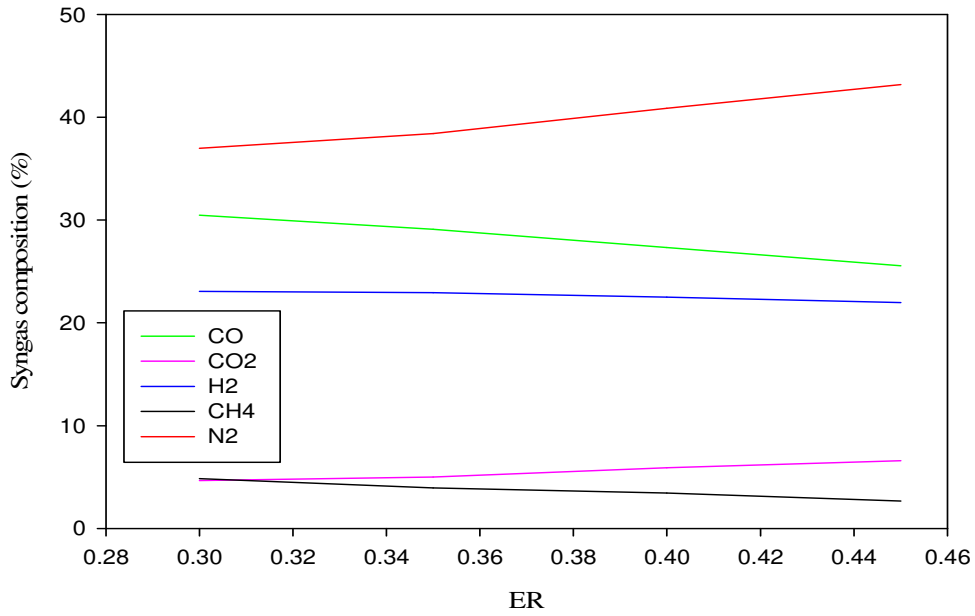

Figure 10. Syngas composition at various ERs

Figure 11 (a) presents the decomposition of volatile matter mass fraction along the downdraft gasifier height at various ER ratios. When biomass enters from the top of the gasifier, due to the heat supplied by the oxidation zone it decomposes from higher molecules to volatile gases, char and tar. Further, the volatile gases reacted with char and converted into final product. Volatile matter decomposition takes place mostly in the pyrolysis zone as Figure 11(a) clearly shows that all the volatile matter decomposed at a distance from 0.6 m to the top (0.96 m) of the gasifier, which is the pyrolysis zone. For the higher ER, the volatile mass

fraction rate is high due to the higher temperature in the oxidation zone. At a lower ER, the volatile mass fraction rate is low, compared to higher ERs.

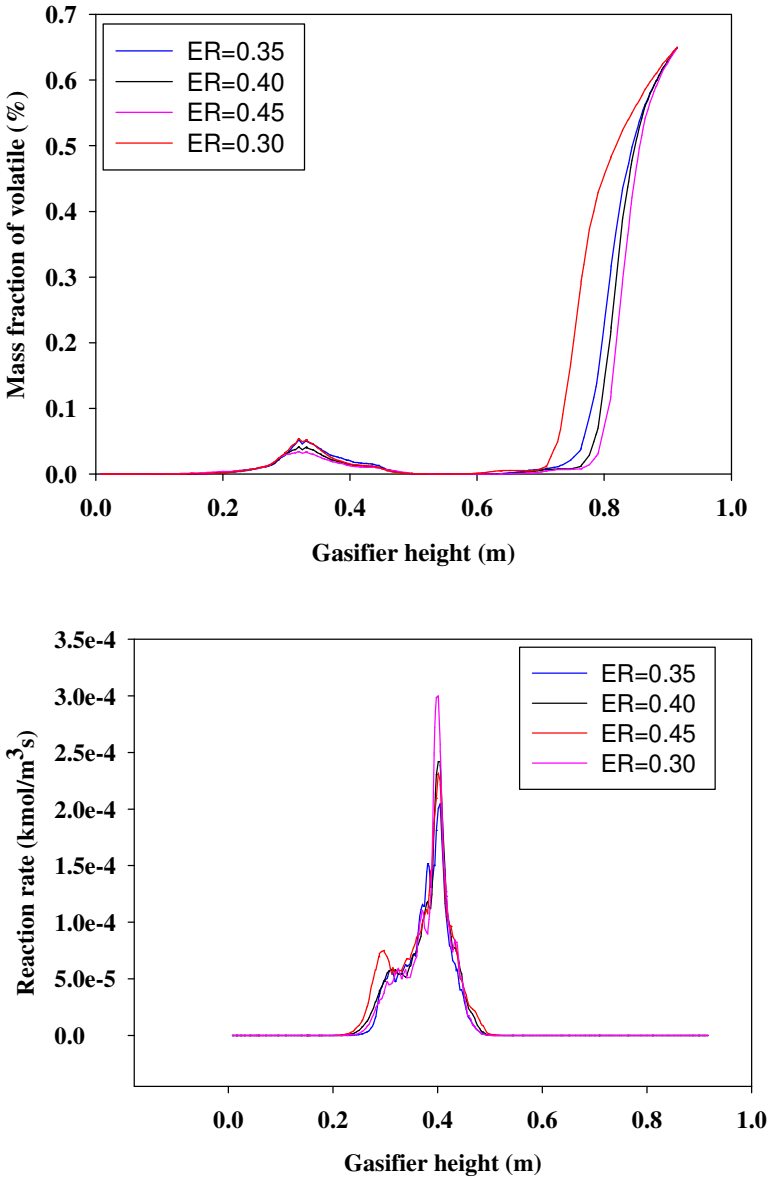

Figure 11. (a) Mass fraction of volatile along the height of gasifier at various ER (top). (b) Reaction rate ($2C+O_2 \rightarrow 2CO$) along the gasifier height at different ER.

Figure 11(b) shows the reaction rate for the combustion reaction at various ERs along the gasifier height. The highest reaction rate is predicted in the oxidation zone for all the ERs. The highest reaction rate is for lower ER and the lowest reaction rate is for higher ER. This is due to the Le Chatelier's principle, which states that higher temperatures favour the formation of reactants in the exothermic reactions and also favour the formation of products through the endothermic reactions.

Figure 12 finally presents the effects of the biomass feeding rate on the syngas production. It can be seen from Figure 12 that the hydrogen concentration decreases while both the carbon monoxide concentration and methane concentration increase with the increasing biomass feed rate.

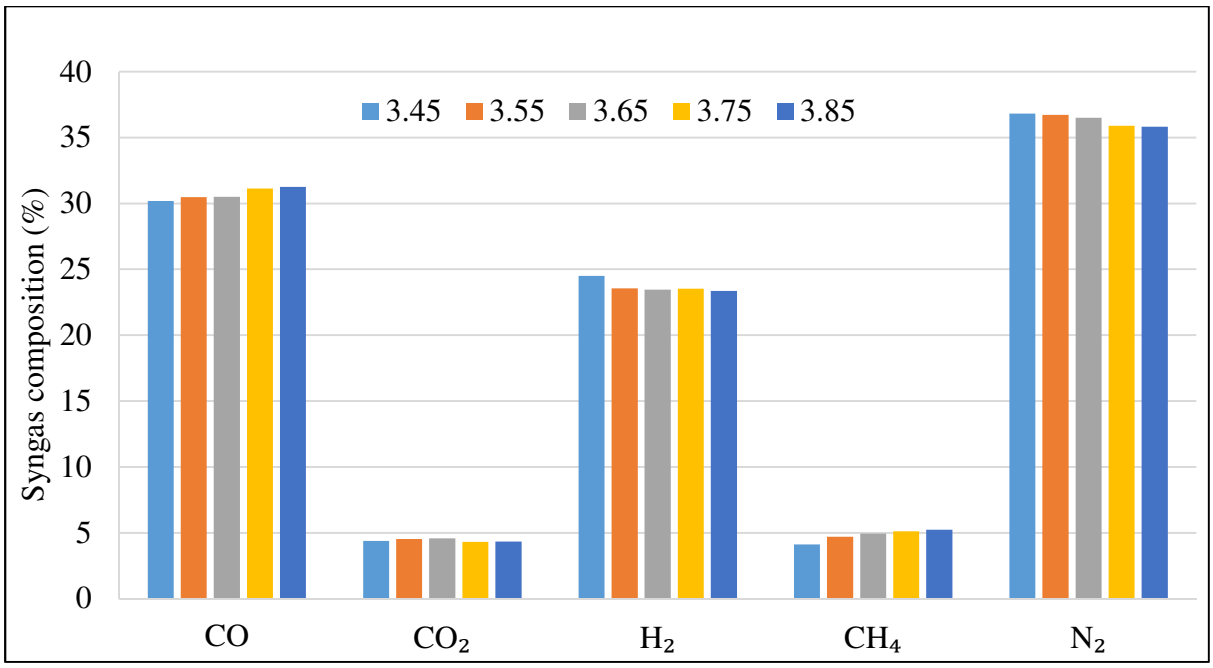

Figure 12. Syngas composition at different biomass feed rates

But carbon dioxide concentration remains almost constant for the various feed rates of rubber wood feedstock. This is due to the fact that when the mass flow rate of biomass for a fixed amount of air mass flow rate is increased, the temperature of gasifier decreases. However, the gasifier temperature as well as the formation of gas concentration in the gasifier is well described through the Le Chatelier's principle mentioned earlier. Therefore, the endothermic reaction (R10) is weaken with the temperature decrease, which further resulted in the decease of H_2 concentration while increasing the CH_4 concentration with the increase of the biomass feeding rate. Moreover, the gas composition of CO is mainly determined through the exothermic reaction R1, thus the lower temperature is favourable for the CO production and consequently, the CO concentration also increases with the increase of biomass feeding rate.

5. Conclusions

A three dimensional computational fluid dynamics (CFD) model was developed to study the gasification of biomass in a downdraft gasifier. Kinetic case study based on the homogeneous combustion reactions was carried out to optimise the gasifier temperature and syngas composition. Model validation was performed by comparing the predicted results of the

gasifier temperature and syngas composition with those of the kinetic model and experimental data. As presented in the paper, the gasification results became very sensitive to the kinetics selection with the occurrence of the highest possible oxidation temperature of 2600K from the reaction parameters utilised in R6.2 (oxidation of H_2). The sensitively study further revealed the optimised kinetic parameters for the homogenous reactions consisting the oxidation of CO (R5), oxidation of H_2 (R6), steam reforming (R7) and methane reforming (R10). The oxidation zone temperature increased again when the equivalence ratio (ER) was increased from 0.3 to 0.45 as prompted by the oxidation reactions. However, when ER increased, carbon monoxide gas composition decreased but carbon dioxide increased. Furthermore, at a higher ER, the volatile release rate became fast compared to that of a lower ER. This model could potentially be used for industrial application for designing and optimising a downdraft gasifier and its syngas production. It could also be extended further by including a detailed tar model [39].

Acknowledgement

We acknowledge Innovate UK (132362, TS/N011686/1) for the research grant support. The second author also acknowledges his RAEng/The Leverhulme Trust Senior Research Fellowship (LTSRF1718\14\45) provided by the Royal Academy of Engineering.

References

[1] Administration USEI. International energy outlook 2016. Energy Information Administration (EIA) (2016).

[2] La Villetta M, Costa M, Massarotti N. Modelling approaches to biomass gasification: A review with emphasis on the stoichiometric method. Renewable and Sustainable Energy Reviews. 2017;74:71-88.

[3] Wang C-H, Zhao D, Tsutsumi A, You S. Sustainable energy technologies for energy saving and carbon emission reduction. Applied Energy. 2017;194:223-4.

[4] Moharamian A, Soltani S, Rosen MA, Mahmoudi SMS, Morosuk T. A comparative thermoeconomic evaluation of three biomass and biomass-natural gas fired combined cycles using organic Rankine cycles. Journal of Cleaner Production. 2017;161:524-44.

[5] Yucel O, Hastaoglu MA. Kinetic modeling and simulation of throated downdraft gasifier. Fuel Processing Technology. 2016;144:145-54.

[6] R.C.Sastry ABa. Biomass Gasification Processes in Downd raft Fixed Bed Reactors: A Review. Internation Journal of Chemical Engineering and Applications. 2011;2:425-33.

[7] Chen C, Horio M, Kojima T. Numerical simulation of entrained flow coal gasifiers. Part I: modeling of coal gasification in an entrained flow gasifier. Chemical Engineering Science. 2000;55:3861-74.
[8] Zainal ZA, Ali R, Lean CH, Seetharamu KN. Prediction of performance of a downdraft gasifier using equilibrium modeling for different biomass materials. Energy Conversion and Management. 2001;42:1499-515.
[9] Melgar A, Pérez JF, Laget H, Horillo A. Thermochemical equilibrium modelling of a gasifying process. Energy Conversion and Management. 2007;48:59-67.
[10] Jarungthammachote S, Dutta A. Thermodynamic equilibrium model and second law analysis of a downdraft waste gasifier. Energy. 2007;32:1660-9.
[11] Huang HJ, Ramaswamy S. Modeling biomass gasification using thermodynamic equilibrium approach. Appl Biochem Biotechnol. 2009;154:14-25.
[12] Patra TK, Sheth PN. Biomass gasification models for downdraft gasifier: A state-of-the-art review. Renewable and Sustainable Energy Reviews. 2015;50:583-93.
[13] Wang Y, Kinoshita CM. Kinetic model of biomass gasification. Solar Energy. 1993;51:19-25.
[14] CD B. Dynamic behaviour of stratified downdraft gasifiers. Chemical Engineering Science. 2000;55:2931-44.
[15] Ong Z, Cheng Y, Maneerung T, Yao Z, Tong YW, Wang C-H, et al. Co-gasification of woody biomass and sewage sludge in a fixed-bed downdraft gasifier. AIChE Journal. 2015;61:2508-21.
[16] Fletcher DF, Haynes BS, Chen J, Joseph SD. Computational fluid dynamics modelling of an entrained flow biomass gasifier. Applied Mathematical Modelling. 1998;22:747-57.
[17] Gerun L, Paraschiv M, Vîjeu R, Bellettre J, Tazerout M, Gøbel B, et al. Numerical investigation of the partial oxidation in a two-stage downdraft gasifier. Fuel. 2008;87:1383-93.
[18] Papadikis K, Gu S, Bridgwater AV. CFD modelling of the fast pyrolysis of biomass in fluidised bed reactors. Part B: Heat, momentum and mass transport in bubbling fluidised beds. Chemical Engineering Science. 2009;64:1036-45.
[19] Xue Q, Heindel TJ, Fox RO. A CFD model for biomass fast pyrolysis in fluidized-bed reactors. Chemical Engineering Science. 2011;66:2440-52.
[20] Liu H, Elkamel A, Lohi A, Biglari M. Computational Fluid Dynamics Modeling of Biomass Gasification in Circulating Fluidized-Bed Reactor Using the Eulerian–Eulerian Approach. Industrial & Engineering Chemistry Research. 2013;52:18162-74.

[21] Wu Y, Zhang Q, Yang W, Blasiak W. Two-Dimensional Computational Fluid Dynamics Simulation of Biomass Gasification in a Downdraft Fixed-Bed Gasifier with Highly Preheated Air and Steam. Energy & Fuels. 2013;27:3274-82.

[22] Kumar U, Salem AM, Paul MC. Investigating the thermochemical conversion of biomass in a downdraft gasifier with a volatile break-up approach. Energy Procedia. 2017;142:822-8.

[23] Salem AM, Paul MC. An integrated kinetic model for downdraft gasifier based on a novel approach that optimises the reduction zone of gasifier. Biomass and Bioenergy. 2018;109:172-81.

[24] ANSYS 15 Fluent Theory Guide. Canonsburg, PA 15317; 2013.

[25] Kumar U, Paul MC. CFD modelling of biomass gasification with a volatile break-up approach. Chemical Engineering Science. 2019, v195, pp413-422.

[26] Jayah TH, Aye L, Fuller RJ, Stewart DF. Computer simulation of a downdraft wood gasifier for tea drying. Biomass and Bioenergy. 2003;25:459-69.

[27] Xie J, Zhong W, Jin B, Shao Y, Liu H. Simulation on gasification of forestry residues in fluidized beds by Eulerian–Lagrangian approach. Bioresource Technology. 2012;121:36-46.

[28] Gómez-Barea A, Leckner B. Modeling of biomass gasification in fluidized bed. Progress in Energy and Combustion Science. 2010;36:444-509.

[29] Dryer FL, Glassman I. High-temperature oxidation of CO and CH_4. Symposium (International) on Combustion. 1973;14:987-1003.

[30] Howard JB, Williams GC, Fine DH. Kinetics of carbon monoxide oxidation in postflame gases. Symposium (International) on Combustion. 1973;14:975-86.

[31] Hottel HC, Williams GC, Nerheim NM, Schneider GR. Kinetic studies in stirred reactors: Combustion of carbon monoxide and propane. Symposium (International) on Combustion. 1965;10:111-21.

[32] Yetter RA, Dryer FL, Rabitz H. Complications of one-step kinetics for moist CO oxidation. Symposium (International) on Combustion. 1988;21:749-60.

[33] Jensen A, Johnsson JE, Andries J, Laughlin K, Read G, Mayer M, et al. Formation and reduction of NOx in pressurized fluidized bed combustion of coal. Fuel. 1995;74:1555-69.

[34] Mitani T, Williams FA. Studies of cellular flames in hydrogen□oxygen□nitrogen mixtures. Combustion and Flame. 1980;39:169-90.

[35] Petersen I, Werther J. Experimental investigation and modeling of gasification of sewage sludge in the circulating fluidized bed. Chemical Engineering and Processing: Process Intensification. 2005;44:717-36.

[36] Jones WP, Lindstedt RP. Global reaction schemes for hydrocarbon combustion. Combustion and Flame. 1988;73:233-49.

[37] Westbrook CK, Dryer FL. Chemical kinetic modeling of hydrocarbon combustion. Progress in Energy and Combustion Science. 1984;10:1-57.

[38] Janajreh I, Al Shrah M. Numerical and experimental investigation of downdraft gasification of wood chips. Energy Conversion and Management. 2013;65:783-92.

[39] Salem, A.M., Kumar, U. and Paul, M.C. Kinetic Modelling for Tar Evolution and Formation in a Downdraft Gasifier. In: World Congress on Engineering 2018, London, UK, 04-06 Jul 2018, pp. 800-804. ISBN 9789881404893